Int. J. Electrochem. Sci., 16 **(2021)** 151018, doi: 10.20964/2021.01.33

International Journal of
ELECTROCHEMICAL
SCIENCE
www.electrochemsci.org

Size Influences of SiO_2-graphene Barrier on the Corrosion Resistance of Epoxy-Acrylic Waterborne Coating

Yifan Shen[1], *Jingxia Yang*[1,2,*], *Shuchuan Wang*[2], *Lingzhi Jing*[1], *Hao Zheng*[1], *Yangyang Du*[1], *Bingjie Zou*[1], *Xuanzheng Lei*[1], *Jingli Xu*[1*]

[1] College of Chemistry and Chemical Engineering, Shanghai University of Engineering Science, LongTeng Road 333, Shanghai201620, P. R. China
[2] T&H chemicals CO. LTD, Tangxi Industrial Zone, Quanzhou Luojiang District, 362011, Fujian, P.R. China
[*]E-mail: yjx09tj@foxmail.com (J. Yang), xujingli@sues.edu.cn (J. Xu)

Received: 19 September 2020 / *Accepted:* 2 November 2020 / *Published:* 30 November 2020

SiO_2-Graphene composited materials can be used as anti-corrosion barriers, which were dispersed in waterborne epoxy-acrylic (EA) resin. Under the same mass of SiO_2 and Gr, the particle size of SiO_2 determines the particle number and surface area, which further influence the coverage of Gr on SiO_2 and their anticorrosion performance. In this research, SiO_2 spheres with three different particle sizes (150, 400, 500 nm) were used to composite with graphene (Gr), and they were linked by bi-functional ligand para-aminobenzoic acid(P), and the designed SiO_2-P-Gr were dispersed in EA resin as anticorrosion barriers, and the influence of SiO_2 particle size is focused. SiO_2-P-Gr barrier can greatly reduce the corrosion current density i_{corr}, from 3.2×10^{-7} A/cm^2 (pure EA coating) to 5.1×10^{-9} A/cm^2 (EA+150nmSiO_2+P+Gr coating), due to the increased resistances for charge transfer (according to EIS fitting) of SiO_2+P+Gr barrier. Especially, 500nmSiO_2-P-Gr exhibited excellent shield in both low and high frequency region according to Bode plot, which may be attributed to the different graphene coverage on the SiO_2 particles with different size under the same mass control.

Keywords: Anti-corrosion; Barrier; Coating; Graphene; SiO_2 sphere

1. INTRODUCTION

Graphene can be used in coatings as a good barrier to prevent the penetration of corrosive media and also block some micropores on the surface of pure resin, which can improve the anticorrosion ability to substrate (e.g. [1-5]). However, graphene is extremely prone to agglomeration, and when it is used in coatings with poor dispersion, it can leads to a decrease in the corrosion resistance of the coatings[6-7]. Therefore, it is important to modify graphene to improve its dispersibility. Generally, the modification of graphene has two approaches: (1) using strong acid/base treatment, to create defects(e.g. COOH[8-

9], NH_2[10]) on graphene surface; (2) grafting functional groups on graphene by linking agents(e.g. KH550[11], bifunctional ligand para-aminobenzoic acid (PABC)[12-13], or alkyne chains[7]), or compositing to other materials (e.g. g-C_3N_4[14]). The second linking approach, especially by PABC, can effectively improve the dispersion of graphene without harsh treatment[12-13]. Previous, we used a kind of modified epoxy resin (EA resin), which grafted acrylate polymer on epoxy chain[12]. The acrylate polymer can introduce hydrophilic carboxyl groups, resulting a water-based epoxy resin with high crosslinking[15]. In this EA resin system, the graphene linked on SiO_2 nanosphere by PABC was added as anticorrosion barrier, and significantly improved the anticorrosive ability of the coating[12]. Nevertheless, previous research only used one kind of SiO_2 sphere, and the influence of graphene amount was not discussed. Both can influence the stacking of the graphene-SiO_2 barrier, resulting in different anticorrosion situation.

In this article, the influence of SiO_2 sphere size and graphene amounts are studied in detail, to see their effects on the corrosion protection in EA resin system. PABC is adopted to connect SiO_2 particles and graphene (SiO_2+PABC+Gr), in which SiO_2 size changes from 150nm to 500nm. Meanwhile, the anticorrosion ability of SiO_2+PABC+Gr was compared with a normal barrier SiO_2+KH550+Gr (linked by silane coupling agent KH550), to confirm the advantage of PABC linking. The anticorrosion properties of the coatings film were characterized by potentiodynamic polarization curves and electrochemical impedance spectroscopy (EIS). Finally, a model is proposed to demonstrate the influence of SiO_2 particle size and graphene under the same mass.

2. EXPERIMENTAL SECTION

Materials: Graphene were received from T&H chemicals Co. LTD, tetraethyl orthosilicate(TEOS), ammonium hydroxide solution and 4-Aminobenzoic acid (P) were bought from Adamas Chemical Co. LTD. Waterborne epoxy resin was supplied by Usolf Co. LTD.

2.1 Synthesis of SiO_2 sphere and Gr-SiO_2 barrier

2.1.1 Preparation of SiO_2 particles

Silica microspheres were prepared by Stober method [16-18], and the parameters for SiO_2 with different size were listed in Table 1. Proper amount of ethyl orthosilicate (TEOS), ethanol (EtOH), DI-water (H_2O) and ammonia (NH_4OH) were added in the three-neck round flasks (with cooling condenser), then the system was sealed by a balloon (to prevent NH_3 from evaporating) and stirred for 2h or 4h.

Table 1. Synthesis Parameters for SiO_2 with different diameters

Sample Name	Diameter (nm)	TEOS (ml)	EtOH (ml)	H_2O (ml)	Ammonia (ml)	Temperature (°C)	time (h)
150nmSiO_2	150	9	480	20	24	40	4
400nmSiO_2	400	60	320	240	160	35	2
500nmSiO_2	500	60	320	240	200	25	2

Along with the reaction time, the solution became cloudy and finally turns into a milky colloidal solution. After the reaction, the solids in the suspension was washed by centrifugation by ethanol for three times. The obtained white precipitation was collected and dried in a vacuum oven at 60℃. Then the dried solid was ground into powder and collected for subsequent modification, named as xnmSiO_2 (x is the diameter).

2.1.2 preparation of graphene-modified silica

0.5g xnmSiO_2 was added into a beaker with 30ml anhydrous ethanol. The suspension was ultrasonically dispersed for 15min. Then 0.4ml ethyl orthosilicate was added and further magnetic-stirred for 15min. After that, 0.274 g PABC was added as linking ligand. After stirring for 15 min, modified-SiO_2 suspension was prepared.

At the same time, 0.005g Gr (1wt% of SiO_2-x) was dispersed into 20ml ethanol by ultrasonic dispersion for 30min, to form Gr-suspension. Then, Gr-suspension was added into above modified-SiO_2 suspension. The mixture was ultrasonically dispersed for 15min and then sheared for 25min with a high-speed shear machine (10000RMP). The solids in the suspension was then collected by centrifugation, and named as xnmSiO_2-P-Gr.

KH550 was used as the ligand for comparison when 500nm-SiO_2 was used, and the synthesis path was the same as above, except that 0.274g PABC was replaced by 0.274g KH550. The sample was named as 500nmSiO_2+K+Gr.

2.2 Preparation of coatings

Water-soluble epoxy-acrylic composite resin was adopted, which was prepared by a chemical grafting method[12, 15].

0.5g SiO_2+P+Gr barrier was added into 50g EA emulsion (30 wt%), and 2-3 drops of defoamer was added. Then the emulsion was dispersed by a high-speed shear machine (10000RMP) for 10 min. Afterwards, curing agent (amino resin) was added while shear machine running. After 5min dispersion, the coating solution was obtained and coated on low carbon steel by a 150μm wire rod coater. The coating was cured at 180℃ for 45min, and aged at room temperature for 5 days before test.

2.3 Characterization

FT-IR was used to monitor the SiO_2 changes before and after Gr-modification using a Perkin-Elmer Spectrum one spectrometer. The morphologies of the SiO_2-Gr barriers were observed using SEM (Hitachi S-8000, Japan) while the coatings surfaces were checked by an upright metallurgical microscope (WMJ-9688 from Shanghai Wumo Optical Instrument Co., Ltd, China).

The corrosion performances of coatings were monitored by an electrochemical workstation (CHI660E, Shanghai Chenhua Device Co., China) using three-electrodes system in 3.5wt% NaCl solution, including potentiodynamic polarization and electrochemical impedance spectroscopes (EIS).

The potentiodynamic polarization was carried out in the range of -0.7~-0.3 V by rate of 0.01V/s, while the EIS results were collected in the range of $1\sim1 \times 10^5$ Hz, using amplitude and 0.005V.

3. RESULTS AND DISCUSSION

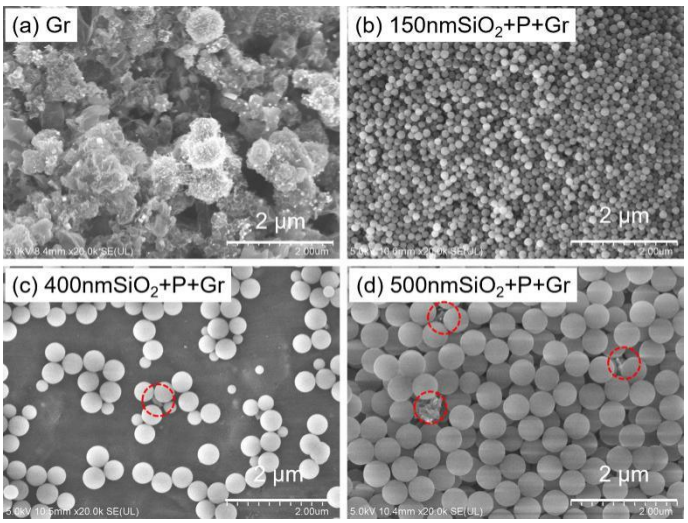

Figure 1. SEM images of Gr and Gr modified SiO_2 spheres with different size

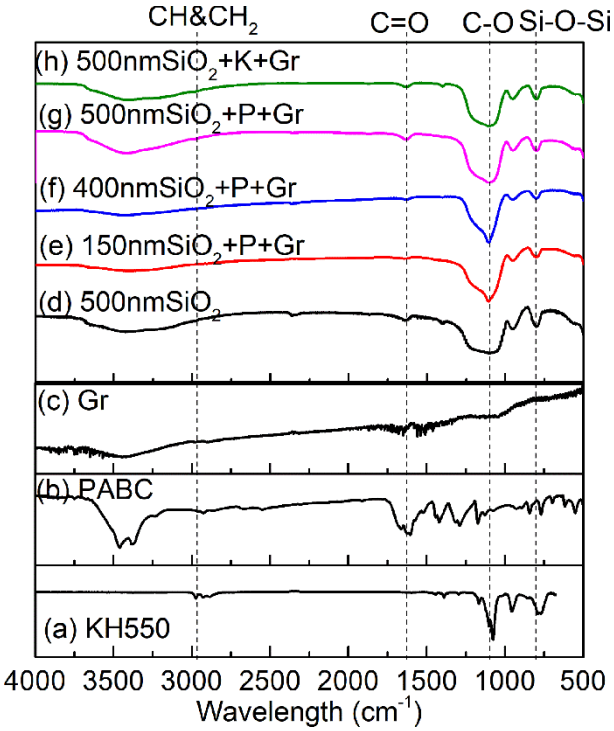

Figure 2. Infrared spectra of graphene modified silica spheres of different particle sizes (a)KH550, (b)PABC, (c)Gr, (d)500nmSiO_2, (e)150nmSiO_2+P+Gr, (f)400nmSiO_2+P+Gr, (g)500nmSiO_2+P+Gr, (h)500nmSiO_2+K+Gr

The SEM image (Figure 1) well reflects the morphology of the connection between graphene and SiO_2 silicon spheres and the dispersion of the modified products. Graphene is a thin lamellar structure, while SiO_2 are sphere particles with different particle sizes of c.a. 150, 400 and 500nm.

It can be observed in Figure 1that there are some graphene lamellar structures in the SiO_2 microsphere structure, especially for 500nmSiO_2+P+Gr sample. Along with the reducing of SiO_2 size, the showing of Gr in the SiO_2+P+Gr is less, which may be related to the surface of SiO_2 particles. As the adding mass of different SiO_2 particles is the same, small particles possesses higher surface than the large one. Thus Gr can cover small SiO_2 particles (e.g. 150nm) better than large particles (e.g. 500nm).

Infrared spectra in Figure 2 demonstrate the change of SiO_2 before and after Gr modification. Compared with the pure 500nmSiO_2(Figure 2d), 500nmSiO_2+P+Gr exhibits an enhanced signal at 1050 cm^{-1}(Figure 2g), corresponding to C-O vibration[19]. As no obvious C-O bond observed in pure PABC ligand(Figure 2b), this enhanced C-O in 500nmSiO_2+P+Gr is caused by Gr(Figure 2c), which may cover or attach on SiO_2 sphere via PABC linking. This has been proved by previous report[12]. The C-O vibrations are even stronger for 150nmSiO_2+P+Gr (Figure 2e) and 400nmSiO_2+P+Gr (Figure 2f), which may be because the coverage of Gr on SiO_2 was higher due to the larger surface area of SiO_2 (relating to smaller particle size). While 500nmSiO_2+P+Gr and 500nmSiO_2+K+Gr are compared, the C-O intensity of 500nmSiO_2+K+Gr (Figure 2h) is inferior to that of 500nmSiO_2+P+Gr(Figure 2g), although KH550 possesses a stronger C-O peak at c.a. 1050 cm^{-1}(Figure 2a) than that of PABC(Figure 2b). This probable also related with the spreading of Gr, and the spreading of Gr by PABC linking is more effective due to the rigid structure of benzoic ring in the PABC ligand.

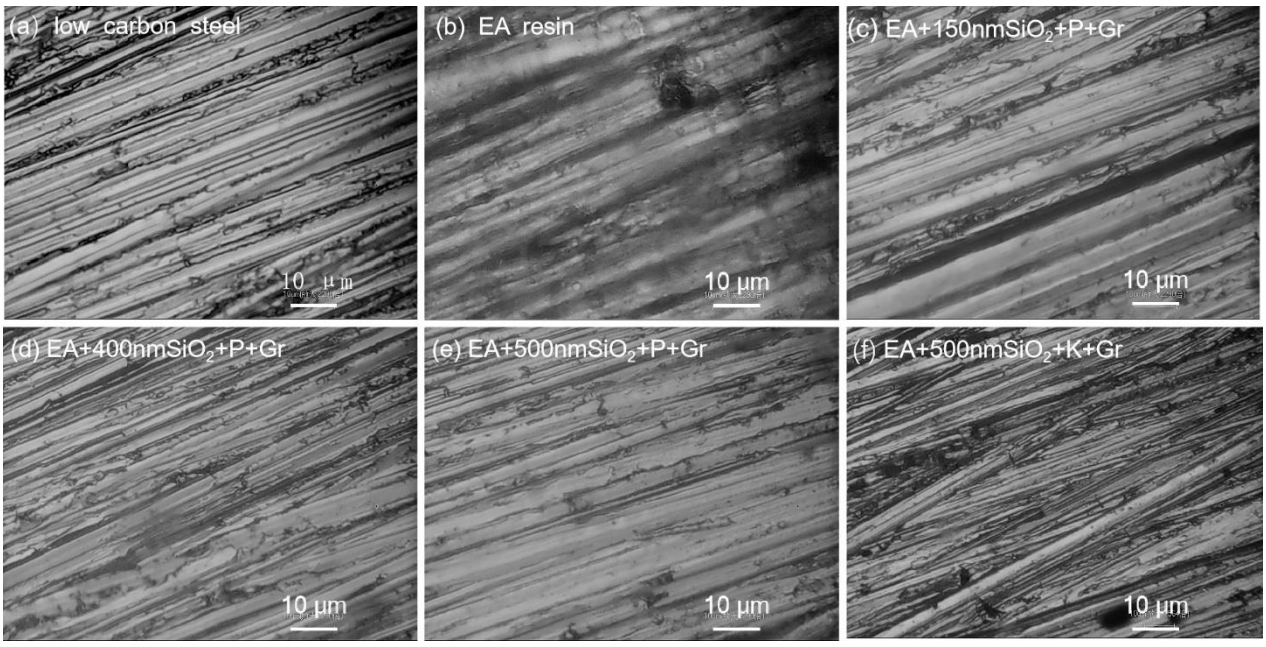

Figure 3. Metallographs of EA coatings with different SiO_2-Gr barriers: (a)low carbon steel, (b)EA resin, (c)EA+150nmSiO_2+P+Gr, (d)EA+400nmSiO_2+P+Gr , (e)EA+500nmSiO_2+P+Gr, (f)EA+500nmSiO_2+K+Gr

The surface of EA coatings with different SiO_2-Gr barriers were observed by metallurgical microscope (Figure 3). As the low carbon steel was polished before using, thus it shows a number of scratches on the surface (Figure 3a). These scratches are still clear after the coating covered, due to the EA resin has good transparency, and no obvious difference can be seen from those coatings with different barriers.

Although no significant change shows on the coating surface, they exhibited different anti-corrosion ability. When potentiodynamic polarization curves of the coatings were checked after they stand in 3.5% NaCl solution for 3h, the coatings with xnmSiO_2-P-Gr barrier exhibit excellent performance compared with others, as shown in Figure 4 and Table 2. While large corrosion current densities (i_{corr}) are observed for low carbon steel (1.8×10^{-6} A/cm^2) and the pure EA coating (3.2×10^{-7} A/cm^2), the EA+150nmSiO_2+P+Gr coating exhibits the lowest i_{corr} of 5.1×10^{-9} A/cm^2, indicating much less pinholes or defects on the EA+150nmSiO_2+P+Gr coating. The EA+400nmSiO_2+P+Gr and EA+500nmSiO_2+P+Gr coatings also express excellent corrosion resistances, which possess i_{corr} of 2.7×10^{-8} and 7.1×10^{-9} A/cm^2, respectively. The EA+500nmSiO_2+K+Gr has a relatively smaller i_{corr} (1.8×10^{-7} A/cm^2) than that of EA+500nmSiO_2+P+Gr, which may be related to the worse dispersion of Gr in 500nmSiO_2+K+Gr, as indicated by IR. Compared with the literature, our samples have excellent anticorrosion performances.

Moreover, the positive shift of corrosion potential (E_{corr}) represents a better impermeability of the coating, which may be related to the passivation effect of graphene [20-21]. The E_{corr} values of EA-xnmSiO_2-P-Gr (-0.405~-0.532 eV) are larger than those of coating EA (-0.603 eV) or EA-500nmSiO_2+K+Gr (-0.628 eV), indicating xnmSiO_2-P-Gr composites can serve well as anti-corrosion barrier.

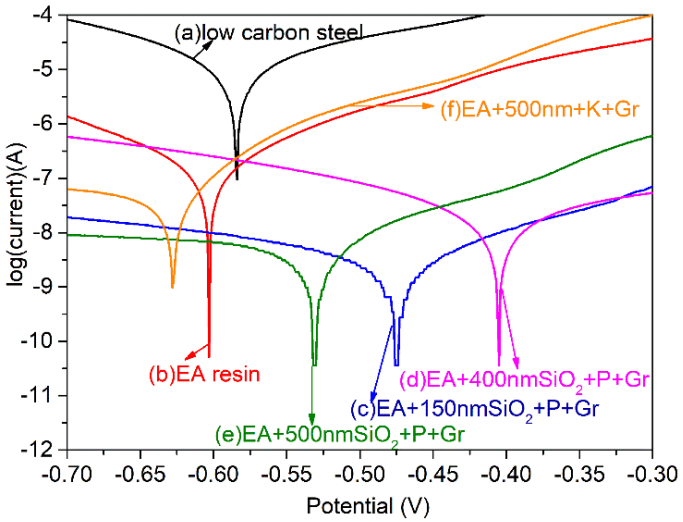

Figure 4. Potentiodynamic polarization curves of composite coatings with different barriers applied to the surface of low carbon steel (a) Pure low carbon steel,(b) with EA resin,(c)EA+150nmSiO_2+P+Gr,(d) EA+400nmSiO_2+P+Gr,(e) EA+500nmSiO_2+P+Gr,(f) EA+500nmSiO_2+K+Gr

EIS can reflect the anti-corrosion ability more effectively[22], as they can indicate the charge transfer resistance(R), as displayed in Figure 5 and Table 3. The Randles-Warburg model was used to fit the Nyquist plots, which can reflect electrolyte solution-R (Rs), coating-R (Rc), charge transfer-R (Rct), and coating capacitance (CPEc)[23]. The important index is Rct, corresponding to the transfer resistance of aggressive species. Compared to R_{ct} of EA+500nmSiO_2+K+Gr (3.34×10^3 Ω·cm^2), the R_{ct} values are much larger for EA+xnmSiO_2+P+Gr coatings (1.19×10^5~4.10×10^5 Ω·cm^2), indicating they have much better corrosion resistance than EA+500nmSiO_2+K+Gr, supported the potentiodynamic polarization results.

Table 2. Electrochemical polarization results of different acrylic coatings after immersion in 3.5 wt% NaCl solution (pH = 7.0) for 3 h.

Sample	E_{corr} (V)	i_{corr} (A/cm^2)	ba (mV/decade)	-bc (mV/decade)	μ($g.m^{-2}.h^{-1}$)
low carbon steel	-0.584	1.8×10^{-6}	194	147	1.85×10^{-1}
EA resin	-0.603	3.2×10^{-7}	108	249	3.33×10^{-3}
EA+150nmSiO_2+P+Gr	-0.474	5.1×10^{-9}	254	195	5.13×10^{-5}
EA+400nmSiO_2+P+Gr	-0.405	2.7×10^{-8}	243	155	2.81×10^{-4}
EA+500nmSiO_2+P+Gr	-0.532	7.1×10^{-9}	631	111	7.24×10^{-5}
EA+500nmSiO_2+K+Gr	-0.628	1.8×10^{-7}	101	270	1.86×10^{-3}
Gr/g-C_3N_4/epoxy (0.5%) [14]	−0.603	6.0×10^{-9}	161.89	163.94	7.00×10^{-5}
β-CD-CeA/MGO[19]	−0.64	6.0×10^{-8}	245	102	/
lGO[24]	-0.42	2.1×10^{-6}	/	/	2.43×10^{-2}
HA-2G[21]	-0.33	9.4×10^{-8}	/	/	1.93×10^{-2}
FG Ni-Gr[25]	-0.153	3.18×10^{-8}	179.31	100.73	3.72×10^{-4}
GO coating (Sample I) [26]	0.049	9.19×10^{-8}	/	/	/
FG-0.5 wt%	-0.338	1.11×10^{-9}	/	/	1.31×10−5
β-CD-ZnA-MGO[27]	−0.59	1.80×10^{-7}	69	166	/

E_{corr} : Corrosion potential; -bc: Cathode polarization slope;
i_{corr} : corrosion current density; μ: corrosion rate;
ba : Anodic polarization slope;

Bode plots can reflect the coating shield more intuitively. While the impedance in high frequency region (HFR) indicates the resistance of interface layer, the impedance in low frequency region(LFR) reflects the capacity of coating shield to corrosion medium[25, 28]. The EA+500nmSiO_2+K+Gr exhibits a lower impedance in both low and high frequencies, evidenced again that this coating is easier to be corroded. Although the i_{corr} and R_{ct} values of EA-xnmSiO_2-P-Gr are similar, the bode plots still display slightly difference for these coatings with different size of SiO_2 particles. EA-150nmSiO_2-P-Gr has the highest LFR-impedance, indicating the it can store more corrosion medium than others and slowing down their speed to the steel substrate. Nevertheless, its HFR-impedance is the lowest one among these samples, suggesting its interface layer has the lowest resistance. On the contrast, EA-500nmSiO_2-P-Gr exhibits a lower LFR-impedance and a higher HFR-impedance than EA-150nmSiO_2-P-Gr, indicating EA-500nmSiO_2-P-Gr has a very high interface resistance. The different performances can be attributed to the xnmSiO_2-P-Gr barrier displayed in EA resin, as shown below.

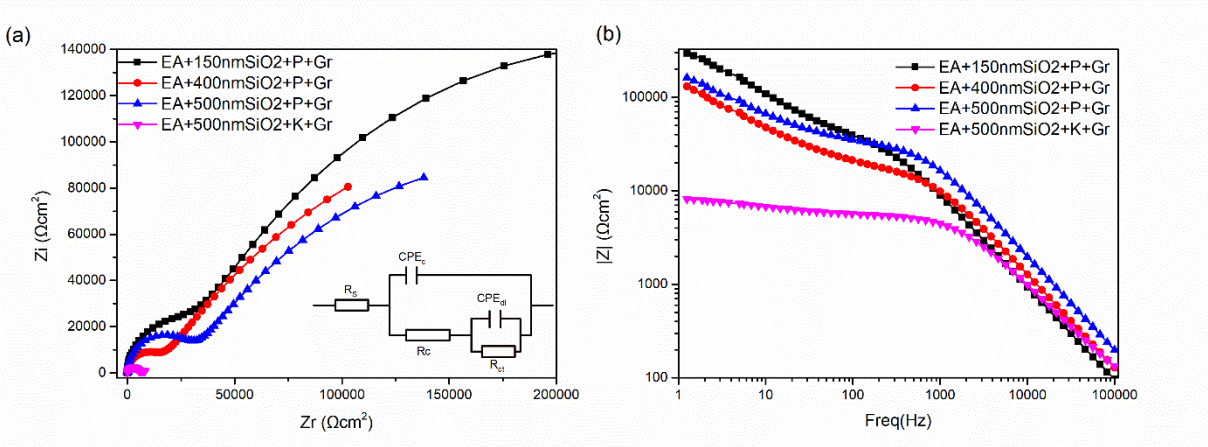

Figure 5. Nyquist plots (a) and Bode impedance plots (b) of EA coatings with different barriers. The fitted equivalent circuit was inserted, which is a Randles-Warburg model.

Table 3. Summary of impedance parameters fitted by the equivalent circuit model

Sample	$R_s(\Omega\cdot cm^2)$	$R_c(\Omega\cdot cm^2)$	CPE_c $(F\cdot cm^{-2})$	$R_{ct}(\Omega\cdot cm^2)$	CPE_{dl} $(F\cdot cm^{-2})$
EA+150nmSiO_2+P+Gr	1.00×10^{-2}	1.03×10^{4}	1.51×10^{-8}	1.19×10^{5}	2.90×10^{-6}
EA+400nmSiO_2+P+Gr	4.32×10^{-3}	1.61×10^{4}	1.24×10^{-8}	4.10×10^{5}	1.64×10^{-6}
EA+500nmSiO_2+P+Gr	4.34×10^{-2}	3.06×10^{4}	8.04×10^{-9}	3.22×10^{5}	8.82×10^{-7}
EA+500nmSiO_2+K+Gr	5.08×10^{1}	5.42×10^{3}	1.77×10^{-8}	3.34×10^{3}	8.36×10^{-6}

The influence of different SiO_2 size on the anti-corrosion ability of the coating was sketched in Figure 6. As displayed in Figure 6a1&2, one 500nmSiO_2 particles has the same mass to thirty-seven 150nmSiO_2 particles, while the surface area of 150nmSiO_2 is about 3.3 times of the surface value of 500nmSiO_2 under the same mass. Thus, when 0.5g SiO_2 mixed with the fixed mass (0.005g) of graphene, the coverage of Gr on the SiO_2 particle would be different. As reported before, PABC can link Gr and SiO2 together though NH_2 and COOH groups. If we assume 0.005g Gr can fully cover the surface of 0.5g 150nmSiO_2, there must be some free Gr, which is still some left after the full coverage of 0.5g 500nmSiO_2 by Gr (Figure 6b1&2), as observed in SEM (Figure 1d). This difference can further influence the performance of anticorrosion. Under the same mass, there are more 150nmSiO_2+P+Gr particles with higher surface than the corresponding 500nmSiO_2+P+Gr, the high surface of 150nmSiO_2+P+Gr thus can store more corrosion medium, yielding the highest LFR-impedance (Figure 6 c1). Nevertheless, more particles possess more channels to diffuse the corrosion medium. Once the storage of corrosion medium reaches the maximum, they will diffuse to the low carbon steel more easily than others, leading to the lowest HFR-impedance of EA+150nmSiO_2+P+Gr coating. The 500nmSiO_2+P+Gr has a totally opposite situation. Although its low surface area cannot keep much corrosion medium (lower LFR-impedance),

the large particle size and the spreading of Gr in the EA resin can reduce the diffusing channels (high HFR-impedance), slowing down the speed of corrosion.

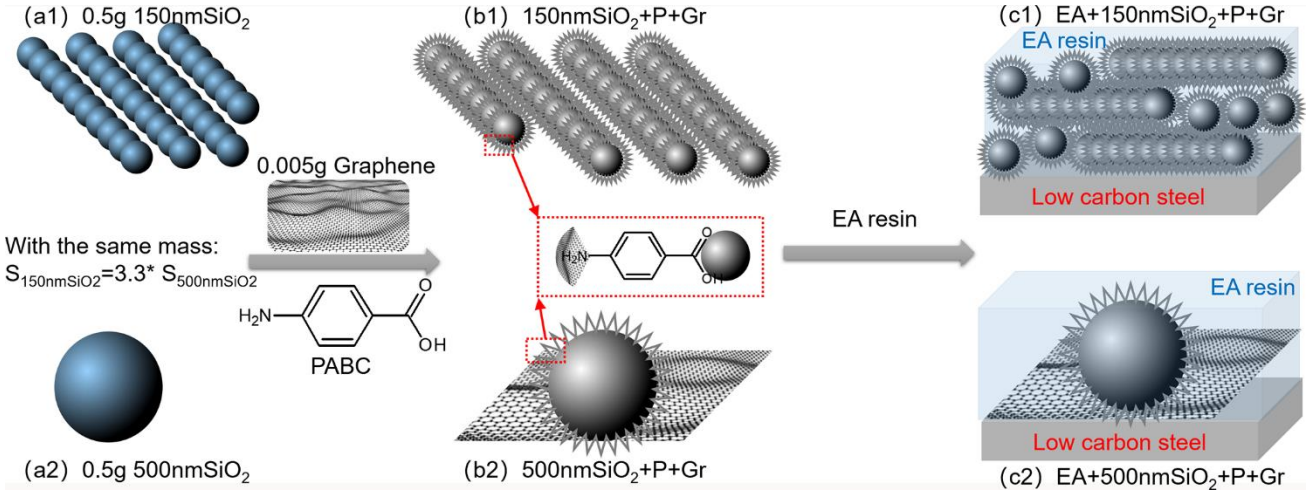

Figure 6. Influence Sketch of SiO2-P-Gr barriers with different particle size on the coating anti-corrosion performance

4. CONCLUSION

Graphene modified SiO_2 was used as anti-corrosion barriers in EA coating, and the diameters of SiO_2 spheres was adjusted in the range of 150-500nm. Bi-functional ligand PABC linked SiO_2-P-Gr composites exhibit better anti-corrosion than the KH550 linked SiO_2-K-Gr composites, due to the rigid structure of benzoic ring in PABC causing an effective spreading of Gr sheet. SiO_2-P-Gr barrier can greatly reduce the corrosion current density i_{corr} and corrosion rate, from 3.2×10^{-7} A/cm^2 (pure EA coating) to 5.1×10^{-9} A/cm^2 (EA+150nmSiO_2+P+Gr coating). Although all xnmSiO_2-P-Gr barriers display very good anti-corrosive performance with increased resistances for charge transfer (according to EIS fitting), the 500nmSiO_2-P-Gr is the best one as the Bode plot proves that it has excellent shield in both low and high frequency region, which may be attributed to the different graphene coverage on the SiO_2 particles with different size under the same mass control.

ACKNOWLEDGEMENT
This work is funded by National Key R&D Program of China (Grant Number 2018YFC1801503), and College Student Research Training Program of SUES (grant number cs1804001). The authors also would like to thank the following persons for preliminary experiments: Yifan Xia, Li Gao, Yunyun Qian and Xiaoyu Zhou.

References

1. D.S. Chauhan, M.A. Quraishi, K.R. Ansari and T.A. Saleh, *Prog. Org. Coat.*, 147 (2020) 105741.
2. A.K. Hussain, I. Sudin, U.M. Basheer and M.Z.M. Yusop, *Corros. Rev.*, 37 (2019) 343.

3. T.D. Nguyen, A.S. Nguyen, B.A. Tran, K.O. Vu, D.L. Tran, T.T. Phan, N. Scharnagl, M.L. Zheludkevich and T.X.H. To, *Surf. Coat. Technol.*, 399 (2020) 126165.
4. Y. Ye, H. Chen, Y. Zou, Y. Ye and H. Zhao, *Corros. Sci.*, 174 (2020) 108825.
5. X. Chen, D. Liao, D. Zhang, X. Jiang, P. Zhao and R. Xu, *Int. J. Electrochem. Sci.*, 15 (2020) 710.
6. J. Lee and D. Berman, *Carbon*, 126 (2018) 225.
7. J.A. Quezada-Renteria, L.F. Chazaro-Ruiz and J.R. Rangel-Mendez, *Carbon*, 167 (2020) 512.
8. M. Krishnamoorthy and N. Jha, *ACS Sustainable Chem. Eng.*, 7 (2019) 8475.
9. J. Sun, J. Ji, Z. Chen, S. Liu and J. Zhao, *RSC Adv.*, 9 (2019) 33147.
10. Y. Tian, Y. Xie, F. Dai, H. Huang, L. Zhong and X. Zhang, *Surf. Coat. Technol.*, 383 (2020) 125227.
11. D. Yu, S. Wen, J. Yang, J. Wang, Y. Chen, J. Luo and Y. Wu, *Surf. Coat. Technol.*, 326 (2017) 207.
12. L. Guo, L. Jing, Y. Liu, B. Zou, S. Hua, J. Zhang, D. Yu, S. Wang, L. Wang and J. Yang, *Int. J. Electrochem. Sci.*, 13 (2018) 11867.
13. H. Li, J. Wang, J. Yang, J. Zhang and H. Ding, *Prog. Org. Coat.*, 143 (2020) 105607.
14. C. Chen, Y. He, G. Xiao, F. Zhong, Y. Xia and Y. Wu, *Prog. Org. Coat.*, 139 (2019) 105448.
15. M. Liu, X. Mao, H. Zhu, A. Lin and D. Wang, *Corros. Sci.*, 75 (2013) 106.
16. W. Stoeber, A. Fink and E. Bohn, *J. Colloid Interface Sci.*, 26 (1968) 62.
17. A. Van Blaaderen and A. Vrij, *Langmuir*, 8 (1992) 2921.
18. M. Zhang, Y. Ling, L. Liu, J. Xu, J. Li and Q. Fang, *Inorganic Chemistry Frontiers*, 7 (2020) 3081.
19. A. Dehghani, G. Bahlakeh and B. Ramezanzadeh, *Chem. Eng. J.* , 400 (2020) 125860.
20. B. Zou, X. Chang, J. Yang, S. Wang, J. Xu, S. Wang, S. Samukawa and L. Wang, *Progress in Organic Coatings*, 133 (2019) 139.
21. S. Singh, K.K. Pandey, A. Islam and A.K. Keshri, *Ceram. Int.*, 46 (2020) 13539.
22. F. Ding, X. Chen, T. Tian, F. Li, D. Wei, P. Zhang and K. Yang, *Mater. Lett.*, 276 (2020) 128249.
23. T. Ge, W. Zhao, X. Wu, Y. Wu, L. Shen, X. Ci and Y. He, *Mater. Des.*, 186 (2020) 108299.
24. S. Ryu, Y.J. Kwon, Y. Kim and J.U. Lee, *Mater. Chem. Phys.*, 250 (2020) 123039.
25. R. Zhang, G. Cui, X. Su, X. Yu and Z. Li, *J. Alloys Compd.*, 829 (2020) 154495.
26. Y. Guo, D. Bian, G. Jiang and Y. Zhao, *Int. J. Electrochem. Sci.*, 14 (2019) 10332.
27. A. Dehghani, G. Bahlakeh and B. Ramezanzadeh, *J. Hazard. Mater.*, 398 (2020) 122962.
28. M. Ramezanzadeh, B. Ramezanzadeh, M. Mahdavian and G. Bahlakeh, *Carbon*, 161 (2020) 231.